WAVE SCATTERING AND SENSING STRATEGIES IN INTERMITTENT TERRESTRIAL ENVIRONMENTS

D. K. Wilson*, D. E. Lawson, D. G. Albert, M. F. Bigl, and D. Finnegan
U.S. Army Engineer Research and Development Center
Hanover, NH 03755-1290

V. E. Ostashev
NOAA Earth System Research Laboratory
Boulder, CO 80305-3328

G. H. Goedecke
New Mexico State University
Las Cruces, NM 88003-8001

ABSTRACT

This research has two main components: (1) a new, wavelet-based cascade model for intermittent (uneven) distributions of objects in terrestrial environments and (2) a complementary analysis of intermittent wave scattering. Taken together, these developments facilitate realistic statistical descriptions of the performance range (uncertainty) associated with sensing and communication systems. The wavelet cascade model uses a simple set of decay processes to generate complex random media with realistic organization of objects in space and time. It is used to recreate the complex geology of the lava flow field around the Amboy Crater, CA, and incorporated into simulations of seismic wave propagation for this site. The simulations reproduce well the signal travel time distributions recorded along a sampling of 864 separate propagation paths.

1. INTRODUCTION

Terrestrial environments, both natural and man-made, often possess complex spatial distributions of objects that are *intermittent* (*uneven*, *irregular*, *bunched*, or *sporadic*). The distribution of volcanic rock in Fig. 1, from the Amboy Crater, CA vicinity, is an example. Besides surface geology, intermittency is exhibited by atmospheric turbulence, weather events, vegetation, animal populations, urban construction, and many other natural and man-made environments. This paper endeavors to provide a consistent, general approach to describing intermittency and its effects on an important Army problem: signal transmission through terrestrial environments. The performance of sensing and communication systems is heavily impacted by the environments in which they operate. Reliance upon such systems will continue to grow with advancement in information collection, distribution, and analysis technologies.

Conventional treatments of acoustic, seismic, and electromagnetic (EM) signal transmission have assumed that heterogeneities (terrestrial objects) responsible for random scattering of the wavefield are evenly distributed in space. This is a significant shortcoming in existing capabilities for characterizing and predicting environmental effects on system performance. Figure 2 depicts how an intermittent medium affects transmission and sensing of waves. Along some signal propagation paths, the waves encounter many scattering objects and signal coherence (a measure of signal randomness, which usually determines the sensing system performance) is strongly degraded. Other paths encounter few scattering objects and thus provide high coherence. Conventional wave scattering theory (Tatarskii, 1971) assumes, in effect, that all paths experience similar scattering. It thus neglects the *range* of possible outcomes and related uncertainty in system performance, which, depending on the environment, can be very significant.

The research described here involves two main components: first, a new, wavelet-based cascade process model for describing intermittent distributions of objects in random media, and second, a complementary description of the effect of the intermittency on signal transmission. Although the discussion emphasizes surface geology and seismic wave propagation, the goal is to formulate a conceptual and statistical model for intermittency and its effects on wave propagation with applicability extending well beyond the geologic domain. In particular, the model is also intended for application to atmospheric turbulence, which, by scattering sound, radio, and optical waves, often plays a key role in the performance of sensing and communication systems. Intermittent signal propagation in urban areas is also a consideration: acoustic or optical sensors may be rendered useless by obstructions in built-up sections, whereas they may produce very clean signals around open areas such as large lawns and parking lots.

This paper is structured as follows. In Sec. 2, we describe the underlying conceptual model for intermittency and its appearance through *cascade processes*, which involve a sequence of self-similar reactions by which one generation of objects is created from the next. Section 3 describes a basis for mathematical construction for random media models, called *quasi-wavelets* (QWs), that is partic-

Report Documentation Page

Form Approved
OMB No. 0704-0188

1. REPORT DATE	2. REPORT TYPE	3. DATES COVERED
DEC 2008	**N/A**	**-**

4. TITLE AND SUBTITLE	5a. CONTRACT NUMBER
Wave Scattering And Sensing Strategies In Intermittent Terrestrial Environments	5b. GRANT NUMBER
	5c. PROGRAM ELEMENT NUMBER
6. AUTHOR(S)	5d. PROJECT NUMBER
	5e. TASK NUMBER
	5f. WORK UNIT NUMBER
7. PERFORMING ORGANIZATION NAME(S) AND ADDRESS(ES) **U.S. Army Engineer Research and Development Center Hanover, NH 03755-1290**	8. PERFORMING ORGANIZATION REPORT NUMBER
9. SPONSORING/MONITORING AGENCY NAME(S) AND ADDRESS(ES)	10. SPONSOR/MONITOR'S ACRONYM(S)
	11. SPONSOR/MONITOR'S REPORT NUMBER(S)

12. DISTRIBUTION/AVAILABILITY STATEMENT
Approved for public release, distribution unlimited

13. SUPPLEMENTARY NOTES
See also ADM002187. Proceedings of the Army Science Conference (26th) Held in Orlando, Florida on 1-4 December 2008, The original document contains color images.

14. ABSTRACT

15. SUBJECT TERMS

16. SECURITY CLASSIFICATION OF:			17. LIMITATION OF ABSTRACT	18. NUMBER OF PAGES	19a. NAME OF RESPONSIBLE PERSON
a. REPORT	b. ABSTRACT	c. THIS PAGE			
unclassified	**unclassified**	**unclassified**	**UU**	**8**	

FIG. 1: Intermittent distribution of volcanic (basaltic) rock in the Amboy Crater vicinity, Mojave Desert, CA. The crater itself is visible on the horizon, in the middle of the picture.

ularly well suited to describing intermittency and cascade processes. Section 4 brings the paper back to the intermittent surface geology shown in Fig. 1: a QW model for the complex, random geology at this site is described, and simulations of seismic wave propagation through this statistical model are compared to seismic observations from a unique experiment that sampled wave propagation along 864 paths.

2. INTERMITTENT CASCADE PROCESSES

A *cascade* process begins with an initial (or *root*) *generation* of objects triggering a reaction by which the next generation is formed. This generation then triggers formation of the next, and so on. The cascade may involve either relatively large objects breaking down (decaying) into smaller ones, or relatively small objects consolidating into larger ones. If the cascade is *self similar*, the transformation from one generation to the next proceeds by application of a scale-independent set of rules. To formulate such scale-independent rules, dimensional quantities (such as sizes of the objects, the duration of the generation, and energy) are normalized in some manner.

Figure 3 illustrates, in two dimensions, a self-similar cascade mechanism used by Frisch et al. (1978) to describe turbulence. The largest eddies (those produced directly by the instability responsible for the turbulence) are space-filling as represented by the initial, solid square. Each time the generational process of decay into smaller eddies is repeated, some portion of space randomly becomes inactive (unoccupied by the smaller eddies). In this particular illustration, 1/4 of the space becomes inactive upon each iteration. This procedure leads to a fractal set (Mandelbrot, 1977; Schroeder, 1991) upon which the dissipation of turbulent kinetic energy into heat takes place (Frisch et al., 1978; Meneveau and Sreenivasan, 1987).

Although the volcanic processes originally responsible for the formation of the Amboy Crater landscape, and subsequent wind and water erosion, are quite different from turbulence, the distribution of basaltic material in Fig. 1 bears a striking resemblance to the later stages of the ran-

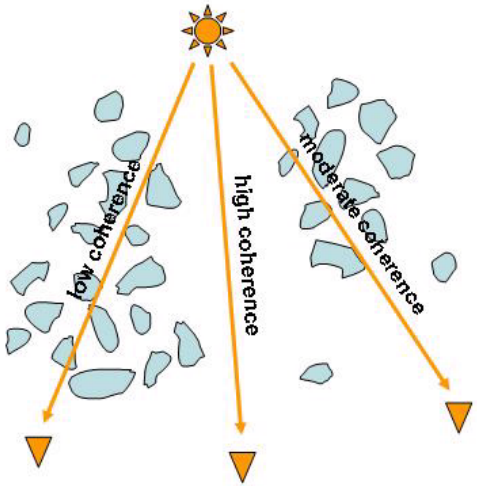

FIG. 2: Interference with propagating waves and sensor performance resulting from an intermittent material distribution.

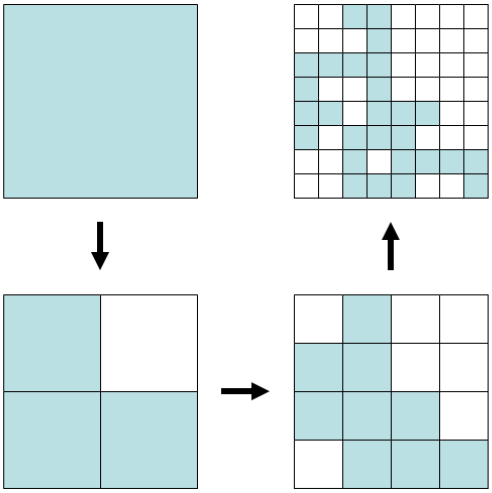

FIG. 3: Notional cascade mechanism used by Frisch et al. to describe intermittent dissipation in turbulence. Each panel indicates a generation of the turbulence. The cascade proceeds counter-clockwise from the upper left. Light blue shading indicates active regions of the turbulence. Repitition of the cascade leads to a fractal set.

dom cascade process depicted in Fig. 3. One might hypothesize that self-similar processes have been or are at work at Amboy; for example, lava ducts may tend to organize in a self-similar fashion (with larger ducts feeding into smaller "fingers"), and erosion breaks down basaltic rocks in a cascade-like fashion. Still, we do not assert that a turbulence cascade model like in Fig. 3 applies literally to past or on-going processes at the Amboy site. Rather, we take the similarity in appearance as evidence that models for intermittent cascade processes might be suitable for describing the geometry of other random, intermittent distributions of objects (such as urban construction, vegetation,

clouds, and the many other terrestrial and galactic phenomena described in Mandelbrot (1977)), even when the link between the cascade process and intermittent geometry is not readily apparent.

Let us thus make several observations about the cascade process depicted in Fig. 3. First, there are certain obvious, unrealistic aspects of Fig. 3 in comparison to the Amboy photograph, Fig. 1. (This is unsurprising, since the original purpose of Frisch et al. (1978) was to explain the formation of a fractal dissipation surface in turbulence, rather than to create visually realistic scenes.) One obvious idealization is the square shape of the objects in the cascade. This may be a problem in wave propagation modeling, for example, when parallel and perpendicular surfaces combine to form artificial waveguides and resonance chambers. Note also in Fig. 3 that the children objects fit together snugly without any overlapping, into the space occupied by the parent object. Such a fit is most easily accomplished with squares and cubes, and requires that the number of children is an integer multiple of the number of parents. In many cascade processes, including turbulence, the children do not possess sharp boundaries and thus must overlap in some sense; they also have an apparently random spatial distribution. The objects usually possess a continuum of sizes, rather than an integer progression. Figure 3 also implies perfect alignment in a temporal sense: all reactions creating a particular object size are synchronous.

Another observation concerns the dynamic nature of the cascades, and how they overlap in space and time. Over time, erosion will break down the rock at the Amboy site, creating smaller objects. Similarly, turbulent eddies decay and are dissipated unless renewed by an instability mechanism such as shear. Thus, the *age* of the cascade is an important consideration. The cascade may be younger (with relatively larger objects) in some regions, and older (with relatively small objects) in other regions. Different parts of the cascade may also proceed at different rates: smaller objects usually break down more quickly than larger ones. This implies the existence of two mechanisms by which the cascade objects can become progressively less space-filling as their size is decreased. The first, illustrated directly in Fig. 3, is that parents do not have enough children to occupy their original space. The second is that subsequent generations are represented by fewer objects, by volume, because they do not survive as long.

With these considerations in mind, we now describe a more general framework for intermittent cascade processes. To start, we define a number of discrete size classes for the objects. The characteristic size (such as the radius or side length of a square) for each class n will be designated as a_n. A smaller index represents larger objects. The ratio $\alpha = a_{n+1}/a_n$ of one size class to the preceding is allowed to take on any value, although it must be independent of n for a self-similar construction.

Next, we formulate a set of *conservative* reactions by which a single parent object, size a_n, breaks down into multiple, smaller objects with sizes $a_{n+1}, a_{n+2}, \ldots$. Each reaction is defined by the number and energies of the children objects it produces. One illustrative reaction is

$$a_n \rightarrow (N_2, \rho_2)\, a_{n+2}. \tag{1}$$

The notation here means that a_n decays into N_2 children objects of size a_{n+2}, each with energy ρ_2 times the energy of the parent object. Conservation of energy requires that $N_2\rho_2 = 1$. The particular case $N_2 = 3$ and $\alpha = 1/\sqrt{2}$ corresponds to the reaction in Fig. 3. When the objects consist of a different material than the background medium, mass-conservation constraints should also be implemented. Other reactions might be defined that produce multiple sizes of children objects, such as

$$a_n \rightarrow (N_1, \rho_1)\, a_{n+1} + (N_3, \rho_3)\, a_{n+3}. \tag{2}$$

This reaction can produce a scale densification; that is, the distribution of object sizes involved in the cascade becomes finer.

How many reactions do we need, and how realistic must they be, to describe a particular, intermittent geometry? Some perspective can be gained from recent developments in agent-based modeling (Bonabeau, 2002), which show that complex group behavior can emerge from a number of autonomous entities obeying simple rules. Thus, it might be suggested that just a few, carefully chosen reactions, for example reactions that lead to cascades with appropriate fractal dimensions and scale densification, will suffice. This idea is demonstrated with an example in Sec. 3.

For self-similar dynamics, the ratio of the lifetime τ_{n+1} of one size class to the preceding must be constant; that is, $\tau_{n+1}/\tau_n = \tau$, where τ is independent of n. The lifetime can be interpreted as the characteristic decay time for completion of a reaction involving a parent with size a_n. Various probabilistic models for the decay may be considered. For present purposes, we adopt the following simple description. After creation, each object of size a_n persists for a time τ_n. One of the R defined reactions then takes place with assigned probability p_r, $r = 1, \ldots, R$. The p_r must sum to 1.

Our description of the reaction is incomplete without a procedure for distributing the objects in space. This procedure actually generates the intermittency, if it exists. Mahrt (1989) has proposed classifying intermittency as *intrinsic* or *global*. Global intermittency is associated with the production mechanism, which in our cascade would be the distribution of the largest (root) generation objects. Intrinsic intermittency is associated with the number density of the children objects relative to the parents. The process illustrated in Fig. 3 is an example of intrinsic intermittency. For the volcanic flow shown in Fig. 1(a), the large patches of rock are associated with global intermittency of the lava flow, whereas cooling, erosion, and other processes subsequent to the volcanic activity tend to produce intrinsic intermittency. In the next section, we will discuss a statistical approach for placing the objects that includes both intrinsic and global intermittency.

3. QUASI-WAVELET MODELING OF INTERMITTENCY

3.1 What are Quasi-Wavelets?

Until this point, the objects in the cascades have not been explicitly described. We now associate them with wavelet, or wavelet-like, functions. Wavelets make convenient analogs for physical objects because they are spatially localized and their mathematical properties are well understood (e.g., Torrence and Compo, 1998). We use the term *quasi-wavelets* (QWs) because, strictly speaking, our objects are not always true wavelets. In particular, restrictions such as a zero mean may be relaxed, and the QWs may be spherically symmetric in multiple dimensions, which is not normal practice in wavelet analysis. Like customary wavelets, QWs are always based on translations and dilations of a parent function; however, their positions and orientations are randomly generated.

Mathematically, the QW is defined by its parent function $f(\xi)$, which we assume here to be spatially symmetric. Here ξ is the magnitude of the vector $\xi \equiv (\mathbf{r} - \mathbf{b}^{nm})/a_n$, $\mathbf{r}$ the spatial coordinate, and $\mathbf{b}^{nm}$ the center position of the QW. The index n indicates the size class of the QW and m a particular QW within that size class. An individual QW comprising a scalar field (i.e., a single field such as temperature) is given by $T^{nm}(\mathbf{r}) = h^{nm}\,\Delta T_n\, f(|\mathbf{r} - \mathbf{b}^{nm}|/a_n)$, where h^{nm} is a random sign factor and ΔT_n is an amplitude factor. The total field is found by summing the contributions of all individual QWs comprising a size class and then summing over the size classes.

We have considered a number of QW parent functions for various applications. Examples are shown in Fig. 4. Three of the illustrated QWs are used to represent scalar fields. To represent a turbulent velocity field, the parent function can be used as a *vector potential*; the velocity field associated with the QW is determined by taking the curl of the potential. Each QW is thus analogous to a turbulent eddy. When the size distribution and rotation rates of the QWs are chosen in a manner consistent with Kolmogorov's hypotheses, turbulence fields with realistic spectral properties result (Goedecke et al., 2004). The velocity QWs can be paired off with scalar, dipole QWs to represent correlated, random fields. In Wilson et al. (2008a), this concept was used to represent the turbulent heat transport above a heated boundary.

3.2 Construction of Intermittent Fields from QWs

Previously, random fields have often been constructed from harmonic functions. The familiar technique involves scaling the amplitudes of the harmonic functions by the square root of the power spectrum, randomizing the phases, and then taking the inverse Fourier transform (Shinozuka and Deodatis, 1996). However, such an approach leads to random fields with smoothly distributed statistical properties: it is not suitable for describing intermittency. This is our main motivation for constructing random fields from QWs instead.

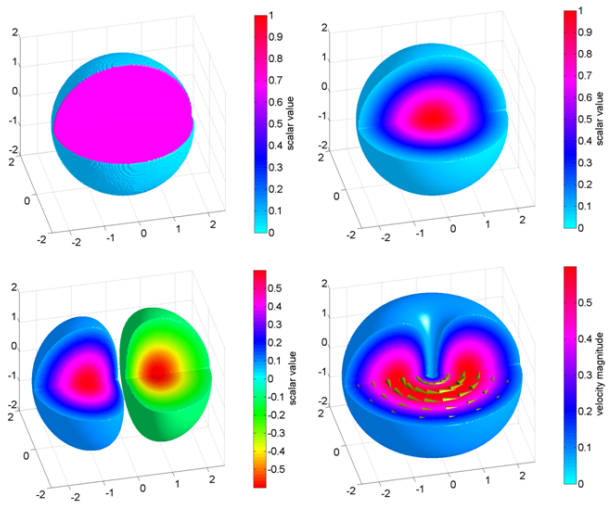

FIG. 4: Images of various 3D quasi-wavelets (QWs). A section of each QW has been cut away to show the interior structure. Top left: Monopole (spherically symmetric) "top-hat" QW. Top right: Monopole Gaussian QW. Bottom left: Dipole derivative-of-Gaussian QW. Bottom right: Rotating (velocity) Gaussian QW.

The basic approach was described in Sec. 2. We propose here a simple, 2D implementation, appropriate to the Amboy site shown in Fig. 1, based on the following three reactions: $a_n \rightarrow (4, 1/4)\, a_{n+2}$, $a_n \rightarrow (2, 2/5)\, a_{n+2} + (1, 1/5)\, a_{n+2}$, and $a_n \rightarrow (1, 1/2)\, a_{n+1} + (4, 1/8)\, a_{n+3}$. Here, the ratio $\alpha = a_{n+1}/a_n$ is set to $1/\sqrt{2}$. The first of these reactions might be considered the "baseline" reaction, which involves decay of an object into four, equal-sized, equal-energy objects. The second produces a spatial fractal distribution and diversification of energy. The third produces diversification of spatial scale. Furthermore, we set the lifetimes to $\tau_n = (4/5)^{n-1}\,\tau_1$, so that smaller objects decay more rapidly. (Note that the actual value of τ_1 is immaterial.) At time τ_n, one of the reactions r will take place with equal probability ($p_r = 1/3$). The objects are represented as solid circles (the 2D version of the QW in Fig. 4, upper left). A recursive MATLAB program was written to simulate the cascade development.

Figure 5 shows a random realization of this cascade process based on a uniformly random spatial placement rule for the children objects; that is, the children are randomly placed anywhere in the domain, thus eliminating the spatial organization. A total of 16 root objects, each with radius 30 m, were placed with uniform, random distribution about the 250 m^2 simulation domain. (An edge region, with width 25 m, is not shown in the figures.) The initiation times (start of the root generation) for the 16 cascades varied randomly between $-\tau_1$ and $+\tau_1$. The random field is shown at time $\tau_1 = 2$, i.e., when most of the cascades are mature.

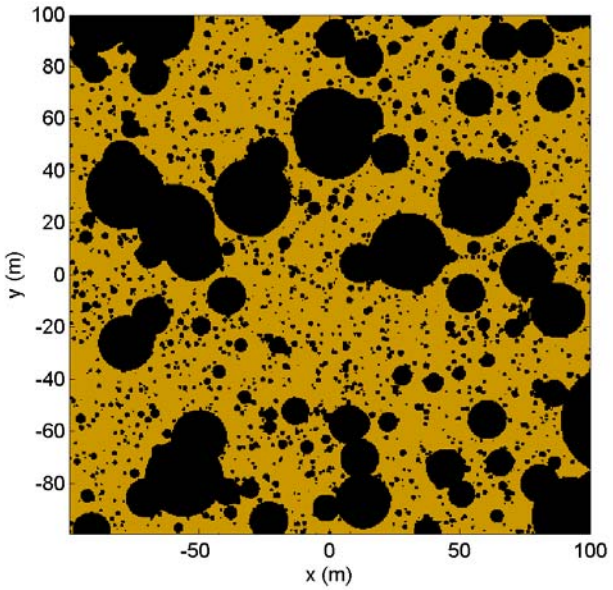

FIG. 5: A random medium constructed from objects (quasi-wavelets) evenly distributed in space. In analogy to the Amboy Crater site, black represents the basaltic rocks (cascade objects); gold is the sand (background medium).

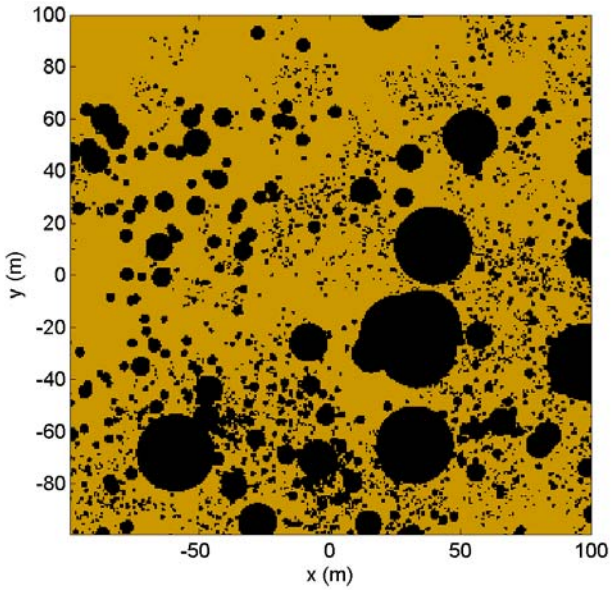

FIG. 6: Same as Fig. 5, except that the objects are distributed in space according to a cascade process including intrinsic intermittency.

Figure 6 was created in the same manner, except that the children objects are placed near to their parents. The center coordinates of the children were selected according to a 2D Gaussian distribution, with standard deviation $2a_n$. Hence, the children fall within a radius $2a_n$ of the parent about 68% of the time. The cascade now has pronounced intermittency, in both intrinsic and global senses. There is also clustering of objects based on their size. This occurs because of the different *ages* of the cascades dominating in different regions.

3.3 Wave Scattering by QWs

We have previously described a theory for wave scattering by QWs (Wilson et al., 2004). The basic idea is to calculate scattering from a single QW, and then, assuming a single-scattering approximation is valid, the scattered fields from all QWs in all size classes can be summed to obtain the total scattering cross section. Recently Wilson et al. (2008b) used QW models as the basis for numerical simulations and analytical formulas of wave propagation through turbulence with intrinsic and global intermittency. The results demonstrate that global intermittency leads to highly non-Gaussian signal statistics for phase fluctuations of acoustic signals. The non-Gaussian statistics have important implications regarding applicability of the conventional theory of wave scattering (e.g., Tatarskii (1971), which is based on Gaussian signal statistics) as well as practical strategies for employing sensors. Practically speaking, signal processing strategies should be based on the recognition that performance of sensing systems consists of periods of good performance disrupted by episodes of dramatically degraded performance. This suggests that "consensus-based" signal processing, as opposed to conventional cross-correlation processing, is most appropriate.

4. GEOLOGIC INTERMITTENCY AND SEISMIC WAVE PROPAGATION

4.1 Amboy Crater Site

As mentioned in the Introduction, we conducted a seismic propagation experiment in the vicinity of the Amboy Crater, which is located in the Mojave Desert near Amboy, CA, about 75 miles east of Barstow. This site was chosen for its highly inhomogeneous geology. The volcanic flow field covers an area of about 70 km^2 and consists primarily of alkali basalt that erupted onto the alluvial plain about 74 to 85 ka (Phillips, 2003). The flow field is composed primarily of vesicular pahoehoe, with a hummocky surface and relief ranging from 2 to 5 m (Parker, 1963). Aeolian (windblown) sand fills the depressions and forms a discontinuous cover over the flow field. Most areas of sand lack vegetation and commonly have irregular, pebble- to cobble-size gravel scattered across their surface. Sand deposits generally range in thickness from a few cm to more than 2 m. The sand at depth greater than $\sim$30 cm is often denser and wet.

The experimental seismic grid (to be described in more detail shortly) was established in a 200 m^2 region of the northwest section of the lava flow field shown in the Fig. 7 satellite image. A high-resolution digital elevation map (DEM) and material classification were developed for the area using a tripod-mounted, scanning lidar, Riegl Model LMS-Z420i. The final DEM (see Fig. 8) was generated

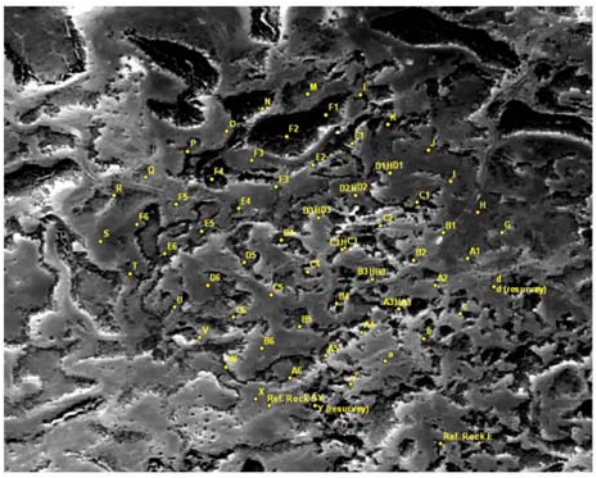

FIG. 7: High-resolution satellite (QuickBird) image of the area containing the seismic test grid. Seismic sensors and shot points are shown in yellow.

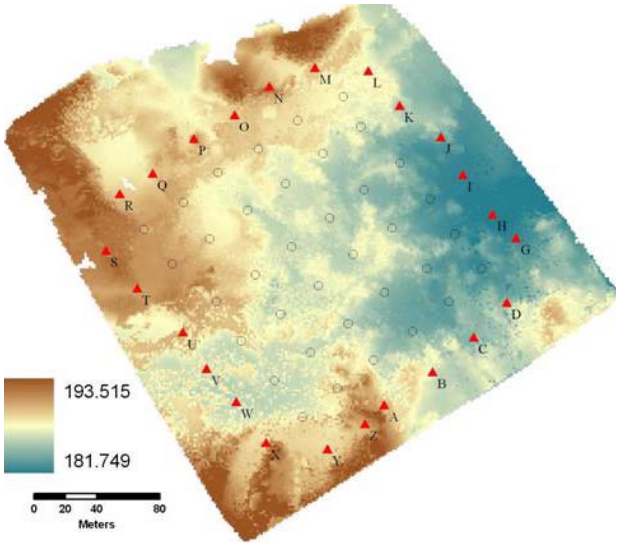

FIG. 8: Digital elevation map for the area containing the seismic grid. Open circles are the geophone locations; triangles are the weight-drop locations.

with 1-m grid spacing. An ISODATA unsupervised classification scheme used the intensity of the lidar returns to map the material types.

4.2 Seismic Measurement Procedure

Thirty-six vertical component geophones (Mark Products L-28 with 4.5-Hz resonance) were installed in a 6-by-6 square grid with 30-m spacing. The geophone locations were adjusted as necessary so they were always inserted into sand. The seismic-wave source was a 16-kg steel sphere dropped from a height of 1.5 m. Twenty-four different source locations around the edge of the sensor grid

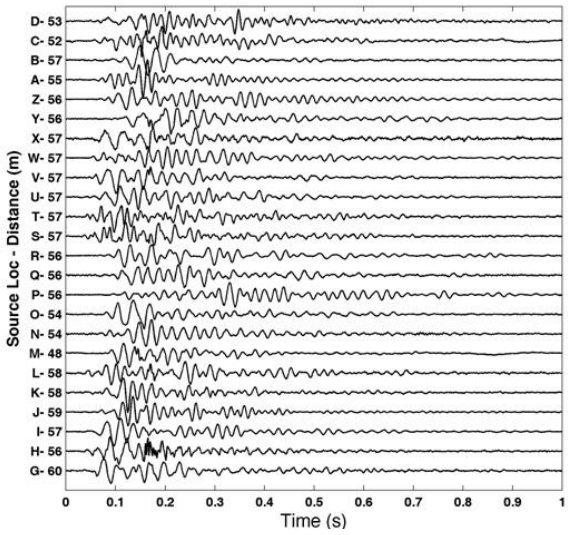

FIG. 9: Signals recorded at the geophones approximately 60-m distant from each of the source locations.

were used as shown in Fig. 8. A geophone located 0.5 m from the impact location triggered the recording system, a Geometrics NZ seismograph. The digital recordings had a 24-bit dynamic range and a sampling rate of 1 kHz.

The 36 geophones and 24 source locations yield 864 propagation paths. Figure 9 shows 2-s time series from a single weight drop at each source location, as recorded by the geophone located (approximately) 60 meters from the source. These measurements show truly remarkable differences for such a short propagation distance and slight location changes. There are large variations in the shape and arrival time of the initial pulse, as well as the envelope of the entire time series and the character of the later arrivals. In some cases, the maximum amplitude is early in the time series (0.1 s) while in others it is delayed up to 0.3 s. The high-frequency arrival at around 0.17 s in some of the traces is likely the acoustic "thump" of the weight impacting the ground.

4.3 Travel-Time Analysis

We now analyze the arrival time distribution of the signal energy. Figure 9 shows that the signal energy arrives at different times along various propagation paths, and is spread over a long time interval. To quantify these effects, we process the signals by first taking the Hilbert transform. The magnitude of the Hilbert transform describes the envelope of the signal, the square of which may be interpreted as the signal energy. The signal energy calculated in this manner is then integrated from the start to end of each 2-s record. The linear trend resulting from background noise was subtracted from the integrated energy.

The results of this analysis are shown in Fig. 10. The figure is a scatter plot of the 10%, 50%, and 90% energy arrival times as a function of the distance between the source

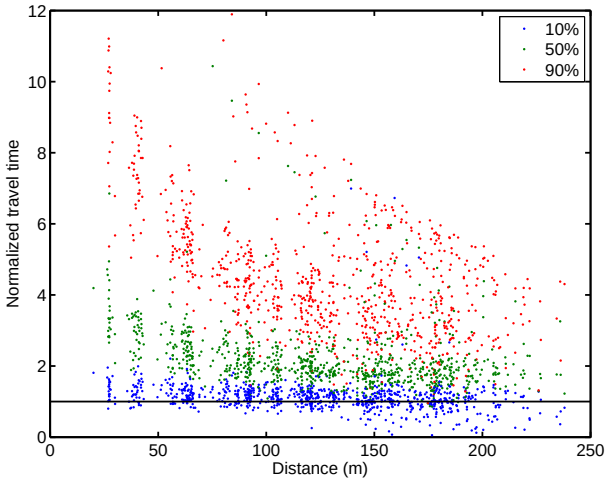

FIG. 10: Scatter plot of signal travel times vs. distance. The travel times are normalized for a propagation speed of 600 m/s as explained in the text. Blue dots are the times at which 10% of the signal energy has arrived, green dots 50%, and red dots 90%.

point and geophone. The times are normalized by dividing by the distance, and multiplying by 600 m/s. This normalization "flattens" the dimensionless time for the 10% arrival time at a value of approximately 1, thus indicating that the early-arriving energy in the recordings travels at about 600 m/s. The normalized plot also makes clear that the *spread* (duration) of the signal energy is relatively larger for *shorter* paths.

Due to the complexity of the site geology and seismic wave propagation in general, interpretation of the signals is not immediately clear. Since P-waves (body compressional waves) travel through basalt at 5400-6400 m/s (Press, 1966), it is unlikely that most of the energy reaching the geophones propagates in this form. The P-wave speed in unsaturated sand varies widely over a range of about 200-1000 m/s (Press, 1966). S-wave (body shear wave) speeds are typically 60% of P-wave speeds; Rayleigh (surface) waves in a half space travel somewhat more slowly than the shear body waves. Given the observed propagation speed of 600 m/s for the early arriving energy, it is reasonable to associate this energy with waves traveling primarily through sand. Since the sand consists of a thin layer with variable thickness, the waves likely interact with both the upper and lower surfaces of the sand and thus are neither purely body nor Rayleigh waves. The typically long delays between the 10% and 90% energy arrival times suggest that the waves are propagating along paths through the sand and reflecting from the basaltic features.

4.4 Comparison to QW Scattering Model

To simulate wave propagation at the Amboy site, we use an acoustic finite-difference, time-domain (FDTD) code. For simplicity, the FDTD code is acoustic in the sense of propagating a single, compressional wave.

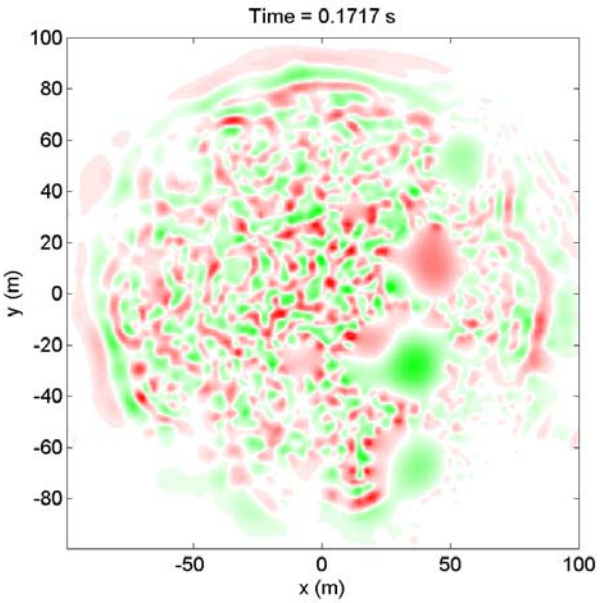

FIG. 11: Finite-difference, time-domain calculation of waves propagating through a random model for the Amboy site. Red is positive pressure; green is negative. (The amplitude is arbitrary.)

Second-order, central finite differencing is used in both space and time. The source is represented by a Ricker wavelet with center frequency 50 Hz. The sandy areas are modeled with a phase speed of 600 m/s and density 1600 kg/m^3. The basalt is modeled with a phase speed of 6000 m/s and density 1900 kg/m^3. Seismic attenuation is included in the calculations by a recursive filter method.

Figure 11 shows the FDTD calculation for the particular random realization of the Amboy site shown in Fig. 6. Shown is the pressure at 0.1717 s after the onset of the initial source signal. Consistent with the seismic traces (Fig. 9), there is very strong, random scattering of the signal. The initial signal, which at 600 m/s travels about 100 m during this time interval, is strongly dispersed and scattered. The longer wavelength within the basalt is evident by the smoother field within the large pieces of basalt.

Normalized travel times (10%, 50%, and 90% energy arrival times, normalized for a propagation speed of 600 m/s as described earlier) were calculated from the simulations by placing receivers at 5-m intervals along radial spokes at 16 different azimuths form the source. Probability density functions (pdfs) for the travel times from the simulation are compared to the experimental data Fig. 12. The pdfs are based on combining all distances between 50 m and 70 m. The mode (pdf maximum) and spread of the arrival times are reproduced quite well by the simulation. Interestingly, the mode for the 50% arrival time is somewhat too low, and that for the 90% arrival time somewhat too high. This may indicate that the wave speed and attenuation need some adjustment. We are presently analyzing in more detail ground-truth data from the site, such as the

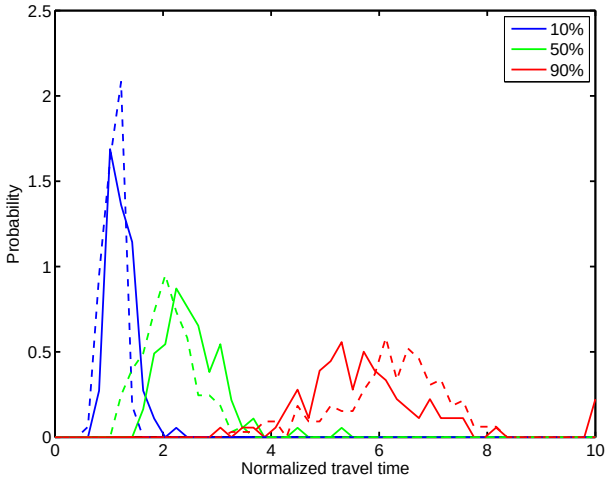

FIG. 12: Probability density functions for the normalized travel times from the Amboy data (solid lines) and FDTD simulation (dashed lines). Distances between 50 m and 70 m are included. Colors indicate the percentage of the total signal energy.

lidar material classifications and sand depth measurements, so as to refine the details of the QW model.

5. CONCLUSION

Random scattering objects in terrestrial environments, such as turbulence, geologic heterogeneities, vegetation, and man-made structures, often impede the performance of Army sensing and communication systems. These objects typically are distributed intermittently (unevenly) in space, thus causing system performance to vary widely from one location to another. By combining fractal cascade processes and wavelets, we have devised a method for constructing random fields with spatial intermittency. The model distributes the originating (root) objects of the cascades through space and time. This is termed *global intermittency*. The cascade process concentrates smaller objects into progressively smaller regions of space. This is *intrinsic intermittency*. Using a cascade model based on a few, simple reactions, we were able to create random media with a qualitative appearance very similar to a site with highly complex geology, namely the Amboy Crater flow field. We then simulated the statistical properties of travel times of waves propagating through this complex environment. Good agreement was found between the observed and simulated travel-time distributions.

ACKNOWLEDGMENTS

Funding was provided by the U.S. Army Basic Research (ASA-ALT) In-House Laboratory Independent Research (ILIR) Program. We thank D. Fisk, S. DeCato, T. Hall, and G. Gooch for their expert help in performing the experiment at Amboy Crater, and B. Tracy for providing the satellite imagery.

REFERENCES

Bonabeau, E., 2002: Agent-based modeling: Methods and techniques for simulating human systems. *Proceedings of the National Academy of Sciences*, **99**, 7280–7287.

Frisch, U., P.-L. Sulem, and M. Nelkin, 1978: A simple dynamical model of intermittent fully developed turbulence. *J. Fluid Mech.*, **87**, 719–736.

Goedecke, G., V. E. Ostashev, D. K. Wilson, and H. J. Auvermann, 2004: Quasi-wavelet model of von Kármán spectrum of turbulent velocity fluctuations. *Boundary-Layer Meteorol.*, **112**, 33–56.

Mahrt, L., 1989: Intermittency of atmospheric turbulence. *J. Atmos. Sci.*, **46**, 79–95.

Mandelbrot, B. B., 1977: *Fractals: Form, Chance, and Dimension*. W. H. Freeman, San Francisco.

Meneveau, C. and K. R. Sreenivasan, 1987: Simple multifractal cascade model for fully developed turbulence. *Phys. Rev. Lett.*, **59**, 1424–1427.

Parker, R. B., 1963: Recent volcanism at Amboy Crater, San Bernardino County, California. Special report, California Division of Mines and Geology. 21 pp.

Phillips, F. M., 2003: Cosmogenic ^{36}CL ages of Quaternary basalt flows in the Mojave Desert, California, USA. *Geomorphology*, **53**, 199–208.

Press, F., 1966: Seismic velocities. In *Handbook of Physical Constants*, S. P. Clark, J., editor, volume 97. Memoirs, Geological Society of America, 97–173.

Schroeder, M., 1991: *Fractals, Chaos, Power Laws*. W. H. Freeman, New York.

Shinozuka, M. and G. Deodatis, 1996: Simulation of multidimensional Gaussian stochastic fields by spectral representation. *Appl. Mech. Rev.*, **49**, 29–53.

Tatarskii, V. I., 1971: *The Effects of the Turbulent Atmosphere on Wave Propagation*. Keter, Jerusalem.

Torrence, C. and G. P. Compo, 1998: A practical guide to wavelet analysis. *Bull. Amer. Meteor. Soc.*, **79**, 61–78.

Wilson, D. K., V. E. Ostashev, and G. H. Goedecke, 2008a: Quasi-wavelet formulations of turbulence and other random fields with correlated properties. *J. Prob. Eng. Mech.*, **accepted**.

Wilson, D. K., V. E. Ostashev, and G. H. Goedecke, 2008b: Sound-wave coherence in atmospheric turbulence with intrinsic and global intermittency. *J. Acoust. Soc. Am.*, **124**, 743–757.

Wilson, D. K., V. E. Ostashev, G. H. Goedecke, and H. J. Auvermann, 2004: Quasi-wavelet calculations of sound scattering behind barriers. *Appl. Acoust.*, **65**, 605–627.